

1 **The influence of spreading rate, basement composition, fluid chemistry and**  
2 **chimney morphology on the formation of gold-rich SMS deposits at slow**  
3 **and ultraslow mid-ocean ridges**

4 Robert D. Knight<sup>1\*</sup>, Stephen Roberts<sup>1</sup>, Alexander P. Webber<sup>1</sup>

5 <sup>1</sup>Ocean and Earth Science, National Oceanography Centre Southampton, University of Southampton,  
6 Waterfront Campus, Southampton, SO14 3ZH, United Kingdom

7 \*Corresponding Author: R.D.Knight@soton.ac.uk

8  
9 **Abstract**

10 Seafloor massive sulphide (SMS) deposits are variably enriched in precious metals including  
11 gold. However, the processes invoked to explain the formation of auriferous deposits do not  
12 typically apply to mid-ocean ridge settings. Here we show a statistically significant, negative  
13 correlation between the average gold concentration of SMS deposits with spreading rate, at  
14 non-sedimented mid-ocean ridges. Deposits located at slow spreading ridges (20-40 mm/a)  
15 have average gold concentrations of between 850-1600 ppb, however, with increasing  
16 spreading rate (up to 140 mm/a), gold concentrations gradually decrease to between ~50-150  
17 ppb. This correlation of gold content with spreading rate may be controlled by the degree and  
18 duration of fluid-rock interaction, which is a function of the heat flux, crustal structure  
19 (faulting) and the permeability of the source rocks. Deposits at ultraslow ridges, including  
20 ultramafic-hosted deposits, are particularly enriched in gold. This is attributed to the higher  
21 permeability of the ultramafic source rocks achieved by serpentinisation and the inherent  
22 porosity of serpentine minerals, combined with relatively high gold concentrations in  
23 peridotite compared with mid-ocean ridge basalt. Variations in fluid chemistry, such as  
24 reducing conditions and the potential for increased sulphur availability at ultramafic-hosted  
25 sites may also contribute to the high concentrations observed. Beehive chimneys, which offer  
26 more favourable conditions for gold precipitation, may be more prevalent at ultramafic-

27 hosted sites due to diffuse low-velocity venting compared with more focussed venting at  
28 basalt-hosted sites.

29

30 *Keywords:* Gold Mineralisation; Massive Sulphide; Mid-Ocean Ridge; Hydrothermal;  
31 Ultramafic

32

### 33 **Introduction**

34 Gold-rich volcanogenic massive sulphide (VMS) deposits and their modern-day equivalents,  
35 seafloor massive sulphide (SMS) deposits, are usually associated with arc, immature back-arc  
36 and rifted environments where felsic lithologies comprise a significant component of the host  
37 rocks (Hannington et al. 1997; Dubé et al. 2007). In these tectonic environments, gold is  
38 enriched by the oxidation of sulphides in the mantle wedge (Mungall 2002) which promotes  
39 the formation of gold-rich magmas (Botcharnikov et al. 2010), and ultimately the addition of  
40 a gold-bearing magmatic fluid to seafloor hydrothermal systems (Yang and Scott 1996,  
41 2006). In comparison, massive sulphide deposits forming at mid-ocean ridge and mature  
42 back-arc spreading centres are typically gold-poor. In these settings, contributions of metal-  
43 rich magmatic fluids are volumetrically insignificant due to the lack of water- and volatile-  
44 rich magmas that are prevalent at convergent margins (Hannington et al. 2005). Gold  
45 concentrations in mid-ocean ridge basalt (MORB) -hosted SMS deposits are typically ten  
46 times lower than defined auriferous VMS deposits (Mercier-Langevin et al. 2011; Patten et  
47 al. 2015). However, some SMS deposits along slow spreading mid-ocean ridges as well as  
48 ultramafic-hosted deposits which typically form along ultraslow spreading ridges, can host  
49 significant gold concentrations of between 850-1600 ppb and 4700-7900 ppb, respectively  
50 (Murphy and Meyer 1998; Mozgova et al. 1999; Munch et al 2001; Bogdanov et al. 2002;

51 Nayak et al. 2014; Fouquet et al. 2010; Webber et al. 2015). These data suggest that the  
52 measured gold concentrations might be related to spreading rate, although this relationship  
53 has not been rigorously tested.

54 Here we show that the average gold concentration of samples collected from SMS deposits  
55 has a statistically significant negative relationship with spreading rate. Furthermore,  
56 ultramafic-hosted deposits, which predominantly form along ultraslow spreading ridges, are  
57 particularly gold-rich. We speculate that this relationship may be due to a range of factors  
58 including the degree and duration of fluid-rock interaction, basement composition, fluid  
59 chemistry and precipitation processes.

60

## 61 **Methods**

62 We have updated and manipulated a pre-existing global geochemical database of SMS  
63 deposits produced by Hannington et al. (2004) with the addition of recently published data  
64 for mid-ocean ridge-hosted SMS deposits (Stepanova et al. 1996; German et al. 1999;  
65 Marques et al. 2006; 2007; Bogdanov et al. 2008; Kristall et al. 2011; Szamalek et al. 2011;  
66 Nayak et al. 2014). Further information was also added from the InterRidge 3.2 database;  
67 e.g., deposit/site name alias(es), ocean basin, region and tectonic setting, latitude and  
68 longitude, host rock(s), whether the site is active or inactive, current maximum temperature,  
69 maximum depth or depth range, and spreading rate where applicable.

70 The data were processed to calculate mean, minimum and maximum values for a suite of  
71 elements for individual deposits. With a focus on gold and cobalt, weighted averages were  
72 calculated, which compensated data that have already been processed to mean values. Values  
73 that fell below the limit of detection were corrected to a value equal to half of the detection  
74 limit for their inclusion in these calculations.

75 In the majority of cases, samples in the database are taken from the surfaces of SMS mounds,  
76 which may be enriched in metals due to zone refining, with an increase in the concentration  
77 of gold with zinc towards the surface of the mounds (e.g., Hannington et al. 1986, 1995;  
78 Petersen et al. 2003). Similarly, massive sulphide chimneys which are naturally metal-rich  
79 are also over-represented. These enriched surface samples are unlikely to be representative of  
80 the deposits in their entirety. However, since there is a great range of gold concentrations  
81 across all deposits that have been sampled in this manner, we assume that the gold  
82 concentration in these surface samples are generally indicative of how gold-rich a deposit is.

83

## 84 **Results**

### 85 *Spreading rate and gold concentration*

86 Minimum, maximum and average gold concentrations for each mid-ocean ridge-hosted SMS  
87 deposit are presented in Table 1. Ultramafic-hosted deposits at slow and ultraslow spreading  
88 ridges record high average gold values of between ~4700-7900 ppb. The highest average gold  
89 concentrations are recorded from the Beebe Vent Field, which is a MORB-hosted deposit  
90 forming along the ultraslow Cayman Rise and will be discussed later in detail. Average gold  
91 concentrations of other MORB-hosted deposits at slow spreading ridges (20-40 mm/a) vary  
92 between ~850-1600 ppb; excluding the MIR zone which is comparable to that of ultramafic-  
93 hosted deposits (3733 ppb). In deposits at intermediate spreading ridges (40-90 mm/a),  
94 average gold concentrations range from ~90-1000 ppb. The majority of deposits have  
95 concentrations of less than ~280 ppb with the Galapagos Rift, Magic Mountain, Source and  
96 the MESO Zone exhibiting higher concentrations of 427, 723, 975 and 1024 ppb,  
97 respectively. At fast spreading ridges (90-140 mm/a), deposits have low average gold  
98 concentrations ranging from ~50-150 ppb. However, at ultrafast spreading sites (>140 mm/a),

99 average gold concentrations of between ~320-580 ppb are observed. All three ultrafast-hosted  
100 deposits are located along the southern East Pacific Rise; EPR 16°43'S, EPR 18°26'S, and  
101 EPR 21°25'S with concentrations of 322, 575 and 413 ppb, respectively.

102 There is a statistically significant relationship, at the 99% confidence interval, between full  
103 spreading rate and average gold concentrations ( $n = 26$ ,  $r = -0.588$ , Fig. 1). As full spreading  
104 rate increases from 20 mm/a to 140 mm/a, the gold content of the associated sulphide  
105 deposits decreases by up to two orders of magnitude. This relationship is exponential in  
106 nature. Grouping the data for each site into their respective categories (i.e., grouping all gold  
107 data for ultramafic, slow, intermediate, fast and ultrafast spreading MORB sites) confirms the  
108 relationship of gold variation with spreading rate (Fig. 2). Kruskal-Wallis tests were  
109 performed on these grouped data and show that there are statistically significant variations  
110 between the medians of these groups at a confidence level of 95 %, except between the slow  
111 and ultrafast spreading groups where there is no significant difference (Table 2). Ultramafic-  
112 hosted deposits associated with ultraslow spreading rates ( $<20$  mm/a) are significantly more  
113 enriched in gold than other MORB-hosted sites, even along slow spreading ridges (Figs. 1-3).  
114 Whilst ultrafast southern EPR sites are not auriferous, they do appear more gold-rich than  
115 predicted by the overall trend (Fig. 2).

116

## 117 **Discussion**

118 There is a negative correlation between the average gold concentration of SMS deposits at  
119 non-sedimented mid-ocean ridges and spreading rate, with ultramafic-hosted deposits at slow  
120 and ultraslow spreading ridges particularly enriched in gold. The processes responsible for  
121 this correlation that require discussion are the degree and duration of fluid-rock interaction,

122 gold content of the source rocks, variation in fluid chemistry, and surface precipitation  
123 mechanisms.

124

125 *Gold enrichment as a function of the degree and duration of fluid-rock interaction*

126 The degree and duration of fluid-rock interaction is critical in determining the quantity of  
127 metals leached from a given lithology (Reed 1997). Provided there is enough time for  
128 hydrothermal fluids to interact with a sufficient source of unaltered rock, greater quantities of  
129 gold may be leached from the crust if gold remains undersaturated in the fluid. Consideration  
130 of the  $^{87}\text{Sr}/^{86}\text{Sr}$  and  $\delta^{18}\text{O}$  signatures of hydrothermal fluids from vent sites along mid-ocean  
131 ridges indicate that hydrothermal fluids from slower spreading ridges are more rock-  
132 dominated compared to those measured at faster spreading ridges (Fig. 4; Bach and Humphris  
133 1999). These rock-dominated signatures in hydrothermal fluids at slow spreading ridges are  
134 the result of greater Sr and O exchange with the oceanic crust which reflects increased  
135 residence time and deeper hydrothermal fluid-flow pathways (Bach and Humphris 1999).  
136 These findings are supported by numerical modelling studies which demonstrate that the  
137 thermal regime at slow spreading ridges is generally cooler (Brown and White 1994) and  
138 hydrothermal fluids require deeper penetration into, and longer residence time within the  
139 oceanic crust to achieve the temperatures typically measured for fluids emanating at  
140 hydrothermal vent sites of 350-400°C (Pelayo et al. 1994). Furthermore, at slow and  
141 ultraslow spreading ridges, tectonic extension often gives rise to low-angle detachment faults  
142 which form oceanic core complexes (e.g., Escartín et al. 2008). These detachment faults  
143 maintain long-lived fluid-flow pathways and support continued convection (Wilcock and  
144 Delaney 1996) as evidenced by the extreme alteration of oceanic rocks along a detachment  
145 fault at 15°45'N near the Mid-Atlantic Ridge (McCaig et al. 2007). Conversely, at fast

146 spreading ridges, episodes of vigorous venting are linked to dyke intrusion events which act  
147 as significant heat sources into the upper crust and increase permeability near the ridge axis  
148 (Wilcock and Delaney 1996). These conditions give rise to shallow, short-lived fluid  
149 circulation and limit the abundance of source rocks available, particularly those that are  
150 unaltered.

151 The degree of fluid-rock interaction may be further enhanced for ultramafic-hosted deposits.  
152 The serpentinisation of ultramafic rocks is accompanied by a volume increase of 25-50%  
153 resulting in episodic fracturing (Schwarzenbach 2016). However, this process should be self-  
154 limiting as the fractures are subsequently filled with serpentine minerals closing fluid-flow  
155 pathways and preventing further serpentinisation and fluid-rock interaction (Macdonald and  
156 Fyfe 1985; O'Hanley 1992; Schwarzenbach 2016). Recent work shows that serpentine and  
157 associated accessory phases form with their own inherent nano-scale porosity, which allows  
158 continued diffusive fluid-flow and pervasive serpentinisation of ultramafic rocks (Tutolo et  
159 al. 2016); possibly resulting in increased leaching of gold from base metal sulphides.  
160 Furthermore, the heat of exothermic serpentinisation reactions may contribute to long-lived  
161 hydrothermal activity at ultramafic-hosted SMS sites (Lowell and Rona 2002; German and  
162 Lin 2004). Therefore, hydrothermal fluids at slow and ultraslow spreading ridges experience  
163 long-lived, deep hydrothermal circulation resulting in greater degrees of fluid-rock  
164 interaction with a greater potential to leach gold from the oceanic crust, particularly where  
165 ultramafic rocks are present.

166

### 167 *Gold content of the source rocks*

168 Differences in source rock composition, particularly between MORB and ultramafic  
169 lithologies, have been shown to exert a control on the composition of the sulphides

170 precipitated at SMS deposits (e.g., Wang et al. 2014; German et al. 2016). The geochemical  
171 characteristics of the host rocks of SMS deposits at mid-ocean ridges are a function of crustal  
172 thickness which varies with spreading and magma supply rates (Bown and White 1994; Niu  
173 and Hékinian 1997). At ridges where the temperature is sufficient to sustain magmatism  
174 capable of developing a full thickness of oceanic crust ( $>20$  mm/a), the host rocks are  
175 typically MORB (InterRidge 3.2 database). However, at ultraslow spreading ridges ( $<20$   
176 mm/a), there is a greater component of tectonic extension and amagmatic spreading via  
177 detachment faulting which exhumes mantle material (e.g., Escartín et al. 2008), in some cases  
178 giving rise to ultramafic-hosted SMS deposits. Furthermore, low magma supply rates also  
179 occur at the termination of ridge sections which may also result in the exhumation of  
180 ultramafic rocks (Fouquet et al. 2010). Ultramafic rocks are partially exhumed in this manner  
181 at the termination of intermediate spreading ridge sections (40-90 mm/a), however, they are  
182 not exposed at the seafloor surface, rather their existence in the sub-seafloor is evidenced by  
183 vent fluids with high  $H_2$  and  $CH_4$  gas contents and sulphide compositions (e.g., at the Kairei  
184 hydrothermal field, Central Indian Ridge; Wang et al. 2014), or by geothermobarometry  
185 indicating that fluid circulation occurs at depths greater than the thickness of the basaltic crust  
186 (Webber et al. 2015).

187 The average concentration of gold in MORB is 0.34 ppb (Webber et al. 2013) whereas the  
188 concentration of gold in peridotites is typically  $>1$  ppb (e.g., Lorand et al. 1999; Luguet et al.  
189 2002; Maier et al. 2012). This is a result of the high partition coefficient for gold between  
190 sulphide and silicate melts of  $\sim 10,000$  (Peach et al. 1990), which causes gold to be retained in  
191 mantle sulphides until relatively high degrees of partial melting (Peach et al. 1990; Naldrett  
192 2011). Therefore, while the degree of fluid-rock interaction may account for the systematic  
193 increase in gold concentrations in SMS deposits with decreasing spreading rate, variations in



194 the gold content of different source rocks may also contribute to the formation of gold-rich  
195 ultramafic-hosted deposits.

196 Further evidence for the leaching of gold from peridotite-hosted sulphides is recognised by  
197 the association of gold with bismuth- and tellurium-bearing minerals in the ultramafic-hosted  
198 Rainbow deposit (Fouquet et al. 2010). These semimetals are likely sourced from mantle  
199 sulphides with gold and the platinum-group elements (PGE). This is supported by PGE  
200 enrichment in ultramafic-hosted SMS deposits, with up to 190 ppb Pt at Rainbow (Bogdanov  
201 et al. 2002) and up to 183 ppb Pt at Logatchev (Mozgova et al. 1999).

202

### 203 *Fluid chemistry*

204 It has been argued that variation in the gold content of the source rocks does not necessarily  
205 explain the differences in gold concentration observed between MORB- and ultramafic-  
206 hosted SMS deposits (Fouquet et al. 2010), with the oxidation state of the hydrothermal fluids  
207 and inputs from metal-rich magmatic fluids the dominant processes in producing gold-rich  
208 SMS deposits (Herzig et al. 1993; Herzig and Hannington 1995; Hannington et al. 2005).  
209 However, these arguments are only relevant for arc- and immature back-arc-hosted deposits  
210 as metal-rich magmatic fluids are volumetrically insignificant at mid-ocean ridges  
211 (Hannington et al. 2005) and the oxidation of hydrothermal fluids may only occur as a result  
212 of the dehydration or partial melting of a subducting slab. Alternative variations in fluid  
213 chemistry must be considered in the formation of gold-rich SMS deposits at mid-ocean  
214 ridges.

215 The transport of gold in high-temperature systems is favoured by acid oxidised fluids and/or  
216 the presence of high-salinity brines (Huston and Large 1989; Hannington et al. 1997). Gold is  
217 transported and concentrated as chloride complexes at high temperatures (>300°C) and

218 precipitated with Cu-Fe-rich sulphides before being subsequently remobilised by late low-  
219 temperature (<250°C) fluids as aqueous sulphur complexes, and concentrated in zinc-rich  
220 polymetallic sulphides along with other elements such as Ag, As, Sb, Hg, and Pb  
221 (Hannington et al. 1986; Herzig et al. 1993).

222 At ultramafic sites, the transport of gold as  $\text{Au}(\text{HS})_2^-$  and  $\text{Au}(\text{HS})^0$  complexes could be  
223 enhanced by reducing conditions and the fact that sulphur may be more readily available.  
224 Alternatively, it has been suggested that abiotic organic complexes (hydrocarbons) may be  
225 important in the transport of gold in ultramafic rocks (Fouquet et al. 2010), however, this has  
226 not been investigated in detail to date.

227 Three SMS deposits along the ultrafast spreading southern East Pacific Rise with relatively  
228 elevated gold concentrations reverse the trend of gold with spreading rates above 140 mm/a.  
229 Notably, these sites, as well as one other southern EPR site (EPR 7°25'S), also have  
230 significantly higher average cobalt concentrations (~978-1321 ppm) than all the other  
231 MORB-hosted deposits (2-494 ppm), as well as most ultramafic-hosted sites (103-465 ppm)  
232 except for Rainbow (3402 ppm; Fig. 5). Phase separation, known to occur along the southern  
233 EPR (Charlou et al. 1996) may be responsible for the elevated concentrations of cobalt and  
234 gold observed. This results in the formation of brines with the capacity to leach gold and  
235 cobalt from the crust as chloride complexes with the latter transported as  $\text{CoCl}_4^{2-}$ , particularly  
236 at temperatures >250°C (Liu et al. 2011; Migdisov et al. 2011).

237

### 238 *Precipitation mechanisms*

239 At mid-ocean ridge vent sites, base and precious metals are precipitated from hot acidic  
240 hydrothermal fluids during mixing with cold circumneutral seawater. However, the nature of  
241 this mixing has implications for the ratio of metals precipitated into the sulphides or lost into

242 the black smoker plume. A study of chimney types at the northern Cleft segment on the Juan  
243 de Fuca Ridge found that chimney type is one of the main controls on fluid mixing and metal  
244 precipitation; zoned tubular Cu-rich chimneys result from focussed high-temperature fluids  
245 (up to 328°C), beehive or diffuser chimneys result from diffuse high-temperature fluids (up to  
246 315°C), and columnar Zn-sulphide-rich chimneys, with narrow channels, result from  
247 focussed low-temperature (261°C) fluid-flow (Koski et al. 1994).

248 Focussed-flow organ-style chimneys which promote the mixing and rapid dilution of metals  
249 in a large volume of seawater is not considered favourable for gold saturation, with >90% of  
250 the fluid metal budget potentially dispersed in the black smoker plume (Fouquet et al. 1993).  
251 In contrast, within beehive chimneys, cooling occurs within the chimney structure and gold is  
252 probably precipitated from  $\text{Au}(\text{HS})_2^-$  complexes at low temperatures (<160°C) along with  
253 sphalerite and pyrite as a result of restricted mixing with seawater at the outer part of the  
254 structure (Fouquet et al. 1993). The increased efficiency of gold precipitation through  
255 enhanced cooling and oxidation of hydrothermal fluids through diffuse venting was also  
256 noted at the TAG deposit, although in this case associated with white smoker venting  
257 (Hannington et al. 1995). However, subsequent zone refining has also concentrated gold and  
258 zinc at the surface of the TAG deposit so the effect of diffuse venting on gold precipitation  
259 cannot be quantified.

260 The formation of beehive chimneys has been linked to lower effusive velocities of the  
261 hydrothermal fluid (e.g., Fouquet et al. 1993; Tivey 1995; Webber et al. 2015). As opposed to  
262 the conical sulphide mounds typically observed at MORB-hosted sites, ultramafic-hosted  
263 SMS deposits are flat and disorganised, which is attributed to poorly focussed diffuse venting  
264 (Fouquet et al. 2010). We speculate that this diffuse, low-velocity venting may give rise to  
265 the formation of more beehive-type chimneys compared with basalt-hosted sites, therefore

266 providing more opportunities for gold to precipitate from the hydrothermal fluid into the  
267 sulphide mound.

268

269 *Case study: The Beebe Vent Field*

270 The Beebe Vent Field (BVF) is a high-temperature black smoker vent site in the Cayman  
271 Trough (Connelly et al. 2012). It is situated 3 km from the spreading centre on a volcanic  
272 mound composed of basaltic pillow lavas, which is part of a spur off the main spreading axis.  
273 The BVF could be considered an end-member vent site for several reasons; it is the world's  
274 deepest known vent site at ~4950 mbsl, venting some of the highest-temperature  
275 hydrothermal vent fluids reported to date (up to 401°C), and it is located on one of the  
276 world's slowest spreading centres with a spreading rate of just 16.9 mm/a. The BVF  
277 comprises several mounds of sulphide, with current high-temperature venting from two areas;  
278 Beebe-125 and Beebe Woods. Both of these sites vent fluid with the same end-member  
279 salinity, indicating that the fluids experience similar sub-surface processes. The primary  
280 difference between the two areas is that Beebe-125 is comprised of tall, slender Cu-rich  
281 chimneys, and Beebe Woods hosts a large cluster of zinc-rich beehive chimneys. Both sites  
282 are gold-rich, but Beebe Woods is significantly richer, containing 19-93 ppm gold (mean =  
283 48.8, n = 8) compared to 0.5-8 ppm (mean = 2.6, n = 5) at Beebe-125. The striking difference  
284 between the gold concentration of the vent sites, and the similarity of the vent fluid  
285 compositions, suggest a strong control on gold content by chimney morphology. The beehive  
286 chimneys of Beebe Woods are highly porous and comprised primarily of laths of pyrrhotite  
287 with pyrite, sphalerite and minor chalcopyrite. This highly reduced mineralogy, together with  
288 high surface area, buffers the fluids close to the pyrite-pyrrhotite buffer, which allows gold  
289 precipitation at ~140°C (Webber et al. 2017). This is supported by the abundance of

290 sphalerite at Beebe Woods, which also precipitates at relatively low temperatures. In contrast,  
291 the slender chimneys of Beebe-125 vent the majority of the fluid at temperatures of ~400°C,  
292 retaining gold in solution.

293 Although surface processes have controlled the abundance of gold at Beebe Woods compared  
294 to Beebe-125, both sites are relatively auriferous, suggesting an underlying cause for high  
295 gold at the BVF. Given an extremely low spreading rate and low melt supply, the fluids  
296 circulating beneath the spreading centre at Beebe may be interacting with ultramafic  
297 lithologies at depth. This is supported by surveys of the canyon walls that describe basalt,  
298 gabbro and peridotite with no clear crustal structure (Stroup and Fox 1981), whilst  
299 geophysics suggests a thin veneer of basalt over gabbro and ultramafic lithologies (ten Brink  
300 et al. 2002). Trace element geochemistry of the BVF sulphides suggests a basement  
301 composition part way between basaltic and ultramafic (Webber et al. 2015). Following this  
302 pervasive interaction with and leaching of gold from ultramafic rocks at depth, the  
303 hydrothermal fluids are then refocussed in the overlying basalt, producing steep, cone-like  
304 sulphide mounds as opposed to flat mounds formed in ultramafic-hosted deposits which  
305 result from diffuse venting over wide areas (Fouquet et al. 2010). The BVF demonstrates that  
306 a combination of sub-surface and precipitation processes have combined to produce a gold-  
307 rich SMS deposit.

308

### 309 **Summary and Conclusions**

310 Average gold concentrations in non-sedimented mid-ocean ridge-hosted SMS deposits show  
311 a negative correlation with spreading rate. Ultramafic-hosted deposits at slow and ultraslow  
312 spreading ridges are particularly gold enriched, and MORB-hosted deposits along slow  
313 spreading ridges may also host significant gold concentrations. Metal-rich magmatic fluids

314 which are used to explain high gold concentrations in arc- and immature back-arc-hosted  
315 deposits (Hannington et al. 1997; Yang and Scott 2006) are volumetrically insignificant at  
316 mid-ocean ridges (Hannington et al. 2005). Instead we suggest that the combined effects of  
317 the degree and duration of fluid-rock interaction, concentration of gold in the source rocks,  
318 fluid chemistry and precipitation mechanisms, all of which can be linked to spreading rate,  
319 control the gold content of SMS deposits.

320 At slower spreading ridges, hydrothermal fluids have deep, long-lived fluid-flow pathways  
321 which is evidenced by the  $^{87}\text{Sr}/^{86}\text{Sr}$  and  $\delta^{18}\text{O}$  signatures of the vent fluids (Bach and  
322 Humphris 1999) and a consequence of low heat flux. At slow spreading ridges (Fig. 6C),  
323 hydrothermal fluids are restricted to interacting with gold-poor source rocks consisting  
324 predominantly of MORB (0.34 ppb Au; Webber et al 2013). However, the longevity of these  
325 hydrothermal cells which remain largely undisturbed by infrequent magmatic activity, and an  
326 abundance of unaltered source rocks leads to the formation of large SMS deposits moderately  
327 enriched in gold.

328 In addition to the above, at ultraslow spreading ridges, hydrothermal fluids forming both  
329 ultramafic-hosted (Fig. 6A) and MORB-hosted (Fig. 6B) SMS deposits, may interact with  
330 more gold-rich ultramafic source rocks (1ppb; e.g., Lorand et al. 1999; Lugué et al. 2002;  
331 Maier et al. 2012) which are susceptible to pervasive alteration given the volume increase of  
332 25-50% associated with serpentinisation resulting in episodic fracturing (Schwarzenbach  
333 2016) and the inherent nano-scale porosity that serpentine and associated accessory phases  
334 possess (Tutolo et al. 2016). The alteration of ultramafic rocks results in reducing conditions  
335 and greater concentrations of sulphur may be available, aiding the transport of gold as  
336  $\text{Au}(\text{HS})_2^-$  and  $\text{Au}(\text{HS})^0$  complexes. At MORB-hosted ultraslow spreading ridges,  
337 hydrothermal fluids may interact with and leach gold from ultramafic lithologies at depth  
338 before being refocussed in the overlying basalt (Fig. 6B).

339 At fast spreading ridges (Fig. 6D), the  $^{87}\text{Sr}/^{86}\text{Sr}$  and  $\delta^{18}\text{O}$  signatures of the vent fluids are less  
340 rock-dominated (Bach and Humphris 1999) suggesting that hydrothermal cells are shallow  
341 due to the emplacement of dykes which act as heat sources in the upper crust and increase  
342 permeability near the ridge axis (Wilcock and Delaney 1996). These shallow hydrothermal  
343 systems which react only with gold-poor MORB are also frequently disrupted by episodic  
344 eruptions leading to the formation of small, gold-poor SMS mounds.

345 Local controls on gold precipitation are evident in the form of sulphide chimney morphology.  
346 Organ-style chimneys focus high-temperature fluids (~350-400°C) which retain >90 % of  
347 their contained metals which are then subsequently lost to the black smoker plume (Fouquet  
348 et al. 1993). Beehive chimneys allow for hydrothermal fluids to be oxygenated and cooled  
349 within the structure of chimneys, resulting in the precipitation of gold at low temperatures  
350 with sphalerite and pyrite (Fouquet et al. 1993; Hannington et al. 1995). Alternatively, the  
351 mineralogy of these beehive chimneys combined with their high surface area may keep the  
352 fluid highly reduced and close to the pyrite-pyrrhotite buffer which raises the temperature at  
353 which gold can precipitate (Webber et al. 2017). We speculate that the diffusive low-velocity  
354 venting associated with slow and ultraslow ultramafic sites that results in the formation of flat  
355 sulphide mounds may also result in the formation of more beehive chimneys, and thus more  
356 sites to support gold precipitation compared to more focussed venting at basalt-hosted sites.

357

### 358 **Acknowledgements**

359 The research leading to these results has received funding from the European Union Seventh  
360 Framework Programme (FP7/2007-2013) under the MIDAS project, grant agreement n°  
361 603418 and NERC grant NE/I01442X/1. We would like to thank one anonymous reviewer  
362 and Editor Bernd Lehmann for their constructive comments that have improved this paper.

364 **References**

- 365 Bach B, Humphris SE (1999) Relationship between the Sr and O isotope composition of  
 366 hydrothermal fluids and the spreading and magma-supply rates at oceanic spreading centers.  
 367 *Geology* 27: 1067-1070
- 368 Bogdanov YA, Bortnikov NS, Vikent'ev IV, Lein AY, Gurvich EG, Sagalevich AM,  
 369 Simonov VA, Ikorsky SV, Stavrova OO, Apollonov VN (2002) Mineralogical-geochemical  
 370 peculiarities of hydrothermal sulfide ores and fluids in the Rainbow Field associated with  
 371 serpentinites, Mid-Atlantic Ridge (36°14'N). *Geol Ore Deposits* 44: 444-473
- 372 Bogdanov YA, Lein AY, Maslennikov VV, Li S, Ul'yanov AA (2008) Mineralogical-  
 373 geochemical features of sulfide ores from the Broken Spur Hydrothermal Vent Field.  
 374 *Oceanology* 48: 734-756
- 375 Botcharnikov RE, Linnen RL, Holtz F (2010) Solubility of Au in Cl- and S-bearing hydrous  
 376 silicate melts. *Geochim Cosmochim Acta* 74: 2396-2411
- 377 Bown JW, White RS (1994) Variation with spreading rate of oceanic crustal thickness and  
 378 geochemistry. *Earth Planet Sci Lett* 121: 435-449
- 379 Charlou JL, Fouquet Y, Donval JP, Auzende JM, Jean-Baptiste P, Stievenard M, Michel S  
 380 (1996) Mineral and gas chemistry of hydrothermal fluids on an ultrafast spreading ridge: East  
 381 Pacific Rise, 17° to 19° (Naudur cruise, 1993) phase separation processes controlled by  
 382 volcanic and tectonic activity. *J Geophys Res* 101: 15899-15919
- 383 Connelly DP, Copley JT, Murton BJ, Stansfield K, Tyler PA, German CR, Van Dover CL,  
 384 Amon D, Furlong M, Grindlay N, Hayman N (2012) Hydrothermal vent fields and  
 385 chemosynthetic biota on the world's deepest seafloor spreading centre. *Nat Commun* 3: 620
- 386 Dubé, B, Gosselin P, Mercier-Langevin P, Hannington M, Galley A (2007) Gold-rich  
 387 volcanogenic massive sulphide deposits, In: *Mineral Deposits of Canada: A Synthesis of*  
 388 *Major Deposit-Types, District Metallogeny, the Evolution of Geological Provinces, and*  
 389 *Exploration Methods*. Geological Association of Canada, Mineral Deposits Division, Special  
 390 *Publication* 5: 75-94
- 391 Escartín J, Smith DK, Cann J, Shouten H, Langmuir CH, Escrig S (2008) Central role of  
 392 detachments faults in accretion of slow spreading oceanic lithosphere. *Nature* 455: 790-794
- 393 Fouquet Y, Cambon P, Etoubleau J, Charlou JL, Ondréas H, Barriga FJAS, Cherkashov G,  
 394 Semkova T, Poroshina T, Bohn M, Donval JP, Henry K, Murphy P, Rouxel O (2010)  
 395 Geodiversity of hydrothermal processes along the mid-Atlantic Ridge and ultramafic-hosted  
 396 mineralization: A new type of oceanic Cu-Zn-Co-Au volcanogenic massive sulfide deposit.  
 397 *Diversity of Hydrothermal Systems on Slow Spreading Ocean Ridges*. *Geophys Monogr Ser*  
 398 188: 321-367



399 Fouquet Y, Wafik A, Cambon P, Mevel C, Meyer G, Gente P (1993) Tectonic setting and  
400 mineralogical and geochemical zonation in the Snake Pit Sulfide Deposit (Mid-Atlantic  
401 Ridge at 23° N). *Econ Geol* 88: 2018-2036

402 German CR, Lin J (2004) The thermal structure of the oceanic crust, ridge-spreading and  
403 hydrothermal circulation: How well do we understand their inter-connections? In: German  
404 CR, Lin J, Parson (eds) *Mid-Ocean Ridges*, American Geophysical Union, Washington, D.C.,  
405 pp 1-18

406 German CR, Hergt J, Palmer MR, Edmond JM (1999) Geochemistry of a hydrothermal  
407 sediment core from the OBS vent-field, 21°N East Pacific Rise. *Chem Geol* 155: 65-75

408 German CR, Petersen S, Hannington MD (2016) Hydrothermal exploration of mid-ocean  
409 ridges: Where might the largest sulfide deposits be forming? *Chem Geol* 420: 114-126

410 Hannington MD, Peter JM, Scott SD (1986) Gold in sea-floor polymetallic sulfide deposits.  
411 *Econ Geol* 81: 1867-1883

412 Hannington MD, Petersen S, Herzig PM, Jonasson IR (2004) A global database of seafloor  
413 hydrothermal systems including a digital database of geochemical analyses of seafloor  
414 polymetallic sulfides. *Geol Surv Canada Open File* 4598

415 Hannington MD, Poulsen KH, Thompson JFH, Sillitoe RH (1997) Volcanogenic gold in the  
416 massive sulfide environment. *Rev Econ Geol* 8: 325-356

417 Hannington MD, de Ronde CEJ, Petersen S (2005) Sea-floor tectonics and submarine  
418 hydrothermal systems. *Econ Geol* 100: 111-141

419 Hannington MD, Tivey MK, Larocque ACL, Petersen S, Rona PA (1995) The occurrence of  
420 gold in sulphide deposits of the TAG hydrothermal field, Mid-Atlantic Ridge. *Can Mineral*  
421 33: 1285-1310

422 Herzig PM, Hannington MD (1995) Polymetallic massive sulfides at the modern seafloor - A  
423 review. *Ore Geol Rev* 10: 95-115

424 Herzig PM, Hannington MD, Fouquet Y, von Stackelberg U, Petersen S (1993) Gold-rich  
425 polymetallic sulfides from the Lau back arc and implications for the geochemistry of gold in  
426 sea-floor hydrothermal systems of the Southwest Pacific. *Econ Geol* 88: 2182-2209

427 Huston DL, Large RR (1989) A chemical model for the concentration of gold in  
428 volcanogenic massive sulfide deposits. *Ore Geol Rev* 4: 171-200

429 Koski RA, Jonasson IR, Kadko DC, Smith VK, Wong FL (1994) Compositions, growth  
430 mechanisms, and temporal relations of hydrothermal sulfide-sulfate-silica chimneys at the  
431 northern Cleft segment, Juan de Fuca Ridge. *J Geophys Res* 99: 4813-4832

432 Kristall B, Nielsen D, Hannington MD, Kelley DS, Delaney JR (2011) Chemical  
433 microenvironments within sulfide structures from the Mothra Hydrothermal Field: Evidence  
434 from high-resolution zoning of trace elements. *Chem Geol* 290: 12-30

- 435 Liu W, Borg SJ, Testemale D, Etschmann B, Hazemann J-L, Brugger J (2011) Speciation and  
436 thermodynamic properties for cobalt chloride complexes in hydrothermal fluids at 35–440°C  
437 and 600 bar: An in-situ XAS study. *Geochim Cosmochim Acta* 75: 1227-1248
- 438 Lorand J-P, Pattou L, Gros M (1999) Fractionation of platinum-group elements and gold in  
439 the Upper Mantle: a detailed study in Pyrenean orogenic lherzolites. *J Petrol* 40: 957-981
- 440 Lowell RP, Rona PA (2002) Seafloor hydrothermal systems driven by the serpentinization of  
441 peridotite. *Geophys Res Lett* 29. doi:10.1029/2001GL014411
- 442 Luguet A, Lorand J-P, Seyler M (2002) Sulfide petrology and highly siderophile element  
443 geochemistry of abyssal peridotites: A coupled study of samples from the Kane Fraction  
444 Zone (45°W 23°20N, Mark Area, Atlantic Ocean). *Geochim Cosmochim Acta* 67: 1553-1570
- 445 Macdonald AH, Fyfe WS (1985) Rate of serpentinization in seafloor environments.  
446 *Tectonophysics* 116: 123-135
- 447 Maier WD, Peltonen P, McDonald I, Barnes SJ, Barnes S-J, Hatton C, Viljoen F (2012) The  
448 concentration of platinum-group elements and gold in southern African and Karelian  
449 kimberlite-hosted mantle xenoliths: Implications for the noble metal content of the Earth's  
450 mantle. *Chem Geol* 302-303: 119-135
- 451 Marques AFA, Barriga FJAS, Chavagnac V, Fouquet Y (2006) Mineralogy, geochemistry  
452 and Nd isotope composition of the Rainbow hydrothermal field, Mid-Atlantic Ridge. *Miner  
453 Deposita* 41: 52-67
- 454 Marques AFA, Barriga FJAS, Scott SD (2007) Sulfide mineralization in an ultramafic-rock  
455 hosted seafloor hydrothermal system: From serpentinisation to the formation of Cu-Zn-(Co)-  
456 rich massive sulfides. *Mar Geol* 245: 20-39
- 457 McCaig AM, Cliff RA, Escartín J, Fallick AE, MacLeod CJ (2007) Oceanic detachment  
458 faults focus very large volumes of black smoker fluids. *Geology* 35: 935-938
- 459 Mercier-Langevin P, Hannington MD, Dubé B, Bécu V (2011) The gold content of  
460 volcanogenic massive sulfide deposits. *Miner Deposita* 46: 509-539
- 461 Migdisov AA, Zevin D, Williams-Jones AE (2011) An experimental study of Cobalt (II)  
462 complexation in Cl<sup>-</sup> and H<sub>2</sub>S-bearing hydrothermal solutions. *Geochim Cosmochim Acta* 75:  
463 4065-4079
- 464 Mozgova NN, Efimov A, Borodaev YS, Krasnov SG, Cherkashov GA, Stepanova TV  
465 Ashadze AM (1999) Mineralogy and chemistry of massive sulfides from the Logatchev  
466 hydrothermal field (14 degrees 45'N Mid-Atlantic Ridge). *Explor Min Geol* 8: 379-395
- 467 Münch U, Lalou C, Halbach P, Fujimoto H (2001) Relict hydrothermal vents along the super-  
468 slow Southwest Indian spreading ridge near 63°56'E – mineralogy, chemistry and chronology  
469 of sulfide samples. *Chem Geol* 177: 341-349
- 470 Mungall JE (2002) Roasting the mantle: Slab melting and the genesis of major Au and Au-  
471 rich Cu deposits. *Geology* 30: 915-918

- 472 Murphy PJ, Meyer G (1998) A gold-copper association in ultramafic-hosted hydrothermal  
473 sulfides from the Mid-Atlantic Ridge. *Econ Geol* 93: 1076-1083
- 474 Naldrett AJ (2011) Fundamentals of magmatic sulphide deposits. In: *Magmatic Ni-Cu and*  
475 *PGE deposits: Geology, geochemistry, and genesis*. *Rev Econ Geol* 17: 1-50
- 476 Nayak B, Halbach P, Pracejus B, Münch U (2014) Massive sulfides of Mount Jourdanne  
477 along the super-slow spreading Southwest Indian Ridge and their genesis. *Ore Geol Rev* 63:  
478 115-128
- 479 Niu Y, Hékinian R (1997) Spreading-rate dependence of the extent of mantle melting beneath  
480 ocean ridges. *Nature* 385: 326-329
- 481 O'Hanley DS (1992) Solution to the volume problems in serpentinization. *Geology* 20: 705-  
482 708
- 483 Patten CGC, Pitcairn IK, Teagle DAH, Harris M (2015) Mobility of Au and related elements  
484 during the hydrothermal alteration of the oceanic crust: implications for the sources of metals  
485 in VMS deposits. *Miner Deposita* 51: 179-200
- 486 Peach CL, Mathez EA, Keays RR (1990) Sulfide melt-silicate melt distribution coefficients  
487 for noble metals and other chalcophile elements as deduced from MORB: Implications for  
488 partial melting. *Geochim Cosmochim Acta* 54: 3379-3389
- 489 Pelayo AM, Stein S, Stein CA (1994) Estimation of oceanic hydrothermal heat flux from heat  
490 flow and depths of midocean ridge seismicity and magma chambers. *Geophys Res Lett* 21:  
491 713-716
- 492 Petersen S, Herzig PM, Hannington MD, Gemmell JB (2003) Gold-rich massive sulphides  
493 from the interior of the felsic-hosted PACMANUS massive sulphide deposits, Eastern Manus  
494 Basin (PNG). In: Eliopoulos D (ed) *Mineral Exploration and Sustainable Development*,  
495 *Proceedings of the 7<sup>th</sup> Biennial SGA Meeting*, Athens, Greece, Millpress, Rotterdam, pp 171-  
496 174
- 497 Reed MH (1997) Hydrothermal alteration and its relationship to ore fluid composition. In:  
498 Barnes HL (ed) *Geochemistry of Hydrothermal Ore Deposits*, 3rd edn. John Wiley, London,  
499 pp. 303-366
- 500 Schwarzenbach EM (2016) Serpentinization and the formation of fluid pathways. *Geology*  
501 44: 175-176
- 502 Stepanova TV, Krasnov SG, Cherkashev GA (1996) Mineralogy, chemical composition and  
503 structure of the MIR mound, TAG hydrothermal field. *Geophys Res Lett* 23: 3515-3518
- 504 Stroup JB, Fox PJ (1981) Geologic investigations in the Cayman Trough: Evidence for thin  
505 oceanic crust along the Mid-Cayman Rise. *J Geol* 89: 395-420
- 506 Szamalek K, Marcinowska A, Nejbort K, Speczik S (2011) Sea-floor massive sulphides from  
507 the Galapagos Rift Zone - mineralogy, geochemistry and economic importance. *Geol*  
508 *Quarterly* 55: 187-202

509 ten Brink US, Coleman DF, Dillon WP (2002) The nature of the crust under Cayman Trough  
510 from gravity. *Mar Pet Geol* 19: 971-987

511 Tivey MK (1995) Modeling chimney growth and associated fluid flow at seafloor  
512 hydrothermal vent sites. In: *Seafloor Hydrothermal Systems: Physical, Chemical, Biological,*  
513 *and Geological Interactions*, 158-177

514 Tutolo BM, Mildner DFR, Gagnon CVL, Saar MO, Seyfried WE (2016) Nanoscale  
515 constraints on porosity generation and fluid-flow during serpentinization. *Geology* 44: 103-  
516 106

517 Wang Y, Han X, Petersen S, Jin X, Oiu Z, Zhu J (2014) Mineralogy and geochemistry of  
518 hydrothermal precipitates from Kairei hydrothermal field, Central Indian Ridge. *Mar Geol*  
519 354: 69-80

520 Webber AP, Roberts S, Murton B, Hodgkinson M (2015) Geology, sulfide geochemistry and  
521 supercritical venting at the Beebe Hydrothermal Vent Field, Cayman Trough. *Geochem*  
522 *Geophys Geosyst*, doi: 10.1002/2015GC005879

523 Webber AP, Roberts S, Murton B, Mills RA, Hodgkinson MR (2017). The formation of gold-  
524 rich seafloor sulfide deposits: Evidence from the Beebe Hydrothermal Vent Field, Cayman  
525 Trough. *Geochem Geophys Geosyst*, doi: 10.1002/2017GC006922

526 Webber AP, Roberts S, Taylor RN, Pitcairn IK (2013) Golden plumes: Substantial gold  
527 enrichment of oceanic crust during ridge-plume interaction. *Geology* 41: 87-90

528 Wilcock WSD, Delaney JR (1996) Mid-ocean ridge sulfide deposits: Evidence for heat  
529 extraction from magma chambers or cracking fronts? *Earth Planet Sci Lett* 145: 49-64

530 Yang K, Scott SD (1996) Possible contribution of metal-rich magmatic fluid to sea-floor  
531 hydrothermal system. *Nature* 383: 420-423

532 Yang K, Scott SD (2006) Magmatic fluids as a source of metals in seafloor hydrothermal  
533 systems. In: Christie DM, Fisher CR, Lee S-M, Givens S (eds) *Back-arc spreading systems:*  
534 *geological, biological, chemical, and physical interactions*, American Geophysical Union,  
535 Washington, D. C. pp. 163-184

536

537

538

539

540

541

542

543

544  
545  
546  
547  
548  
549  
550  
551  
552  
553  
554  
555  
556  
557  
558  
559  
560  
561  
562  
563  
564  
565  
566  
567  
568  
569  
570  
571  
572  
573  
574  
575  
576  
577  
578  
579

Table Captions:

Table 1. Table showing mean, minimum, and maximum gold concentrations for SMS deposits at ultraslow-slow, intermediate, fast, and ultrafast spreading mid-ocean ridges. Those at ultraslow-slow spreading ridges are subdivided into ultramafic- and MORB-hosted deposits.

Table 2. Table showing gold data from mid-ocean ridge-hosted deposits grouped into categories based on spreading rate (slow, intermediate, fast, and ultrafast) with ultramafic-hosted sites grouped separately. P-values derived from Kruskal-Wallis tests between the different groups are also provided. With values  $<0.05$  these data show that the difference between the group medians is significant with a confidence level of 95%.

Figure Captions:

Figure 1: Mean gold concentrations of SMS deposits at non-sedimented mid-ocean ridges (including MORB- and ultramafic-hosted sites) plotted as a function of spreading rate. An exponential trendline shows a significant correlation with an R value of -0.588.

Figure 2. Box and whisker plot showing gold concentrations of ultramafic- and MORB-hosted SMS deposits grouped into ultramafic, slow, intermediate, fast, and ultrafast categories as a function of spreading rate. Boxes show 25th-75th percentile including median line, whiskers show 10th-90th percentile and outliers have been omitted for clarity.

Figure 3. Box and whisker plot showing gold concentrations of ultramafic- and MORB-hosted SMS deposits as a function of spreading rate. Boxes show 25th-75th percentile including median line, whiskers show 10th-90th percentile and outliers have been omitted for clarity.

Figure 4. A) The fraction of Sr in vent fluids that is derived from seawater, and B)  $\Delta^{18}\text{O}$  (the difference between  $\delta^{18}\text{O}$  values of hydrothermal vent fluids and  $\delta^{18}\text{O}$  of local seawater) plotted against full spreading rate (redrawn from Bach and Humphris 1999). Open circles represent average values for individual spreading segments; bars show range of values. Bold lines are regression lines through average values. Thin stippled lines mark error bounds (95%)

580 significance level) of the regression lines. See Bach and Humphris (1999) for full explanation  
 581 and abbreviations.

582 Figure 5. Average cobalt concentrations of ultramafic- and MORB-hosted SMS deposits as a  
 583 function of spreading rate.

584 Figure 6. Schematic diagram summarising how the combined effects of the degree and  
 585 duration of fluid-rock interaction, and the concentration of gold in the source rocks result in  
 586 the formation of; A) large, Au-rich ultramafic-hosted deposits along ultraslow spreading  
 587 ridges; B) large, Au-rich MORB-hosted deposits along ultraslow spreading ridges, C) large,  
 588 moderately Au enriched MORB-hosted deposits along slow spreading ridges, and D) small,  
 589 Au-poor MORB-hosted deposits along fast spreading ridges.

590

591

592 Tables:

593 Table 1.

Full Spreading Rate (mm/a)	Deposit Name	Gold Concentrations (ppb)			No. of Analyses
		Mean	Min	Max	
Ultraslow-slow spreading ridges					
	<i>Ultramafic-hosted</i>				
9.6	<b>Mount Jourdanne</b>	4705	0	12500	21
20.6	<b>Rainbow Field</b>	5342	1530	12100	6
25.5	<b>Logatchev</b>	7893	100	56000	55
	<i>MORB-hosted</i>				
16.9	<b>Beebe Vent Field</b>	17096	458	93600	29
22.9	<b>Broken Spur</b>	1577	8	5580	15
23.6	<b>Mir Zone</b>	3733	42	22600	52
23.6	<b>Alvin Zone</b>	854	680	1020	7
23.6	<b>TAG Mound</b>	971	<5	42960	439
24.1	<b>Snake Pit</b>	1575	<20	10739	100
Intermediate spreading ridges					
47.0	<b>MESO Zone</b>	1024	200	6000	24
55.9	<b>North Cleft</b>	241	30	510	20
55.9	<b>South Cleft</b>	93	<100	130	3
56.0	<b>Source</b>	975	13	2060	6
56.2	<b>High-Rise Field</b>	279	<5	1130	46
56.2	<b>Mothra Field</b>	115	<2	570	202
56.2	<b>Clam Bed</b>	122	20	336	5
56.2	<b>Main Endeavour Field</b>	148	<2	1620	85
56.3	<b>Magic Mountain</b>	723	21	3757	51
61.8	<b>EPR, 21 N</b>	123	<200	480	24
63.0	<b>Galapagos Rift, 85°50'W</b>	427	0	7240	122

Fast spreading  
ridges

95.8	<b>EPR, 11°30'N</b>	133	1	649	10
99.4	<b>Feather Duster</b>	153	5	287	11
136.6	<b>EPR, 7°25'S</b>	47	1	88	13

Ultrafast spreading  
ridges

146.1	<b>EPR, 16°43'S</b>	322	1	1020	19
147.0	<b>EPR, 18°26'S</b>	575	160	1200	14
148.7	<b>EPR, 21°25'S</b>	413	100	680	12

594

595

596

597

598 Table 2.

	Ultramafic	Slow	Intermediate	Fast	Ultrafast
No. of Analyses	76	525	588	34	45
Mean Au ppb	6708	2380	301	107	425
Median Au ppb	4860	430	133	72	370
Kruskal-Wallis test p-values					
Ultramafic	N/A	1.655E-17	1.809E-36	1.675E-15	3.795E-14
Slow		N/A	1.154E-34	5.799E-11	0.1541
Intermediate			N/A	4.776E-04	8.562E-07
Fast				N/A	5.243E-08
Ultrafast					N/A

599

600

601

602

603

604

605

606

607

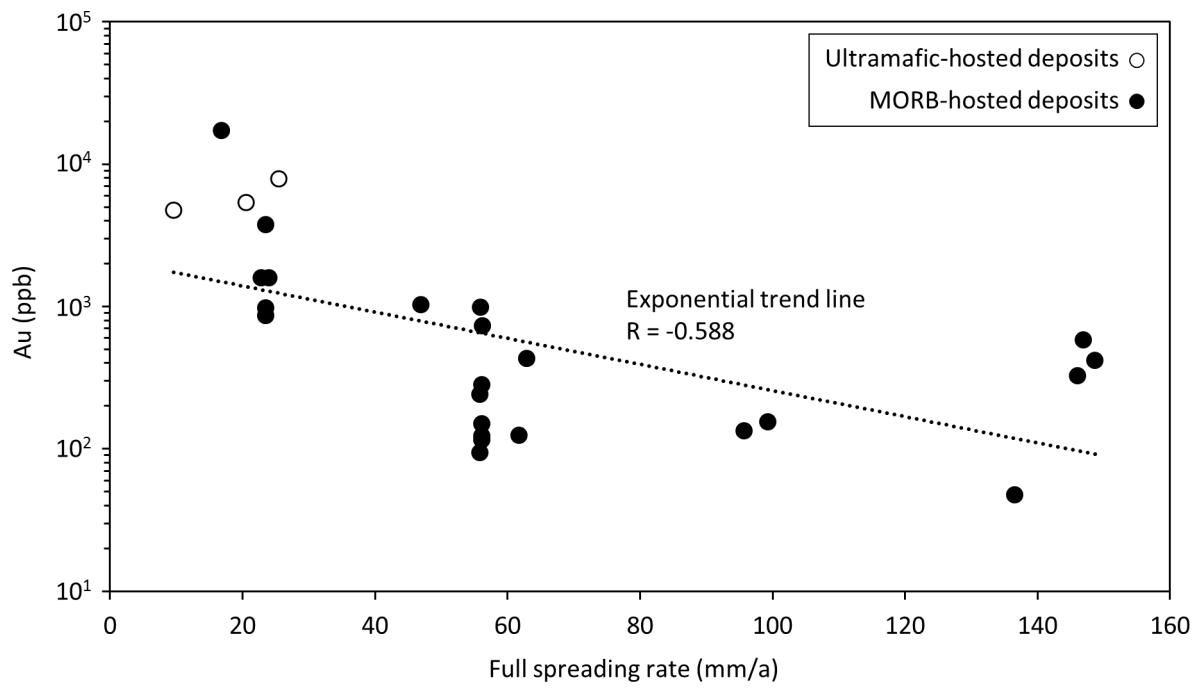
608

609

610

611  
612  
613  
614  
615  
616  
617  
618  
619  
620  
621

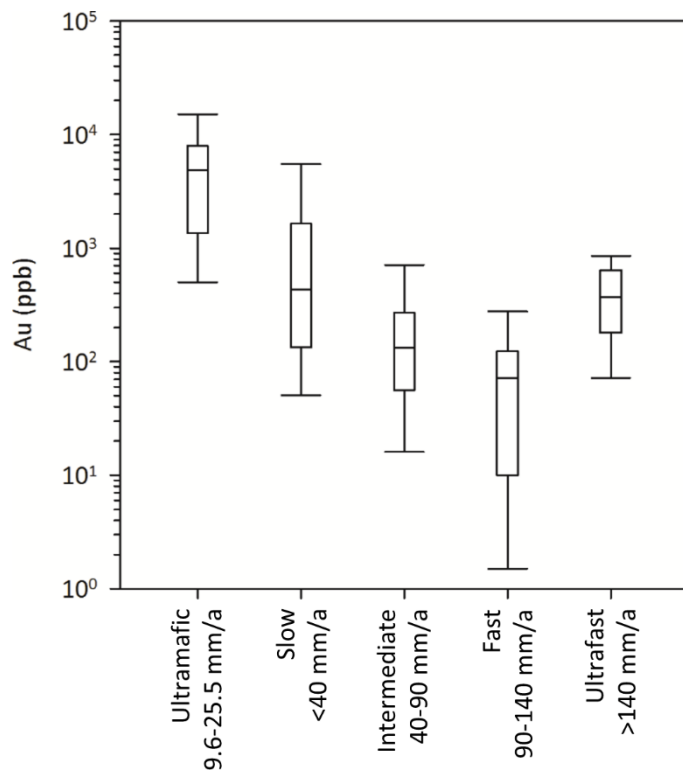
Figure 1



622  
623  
624

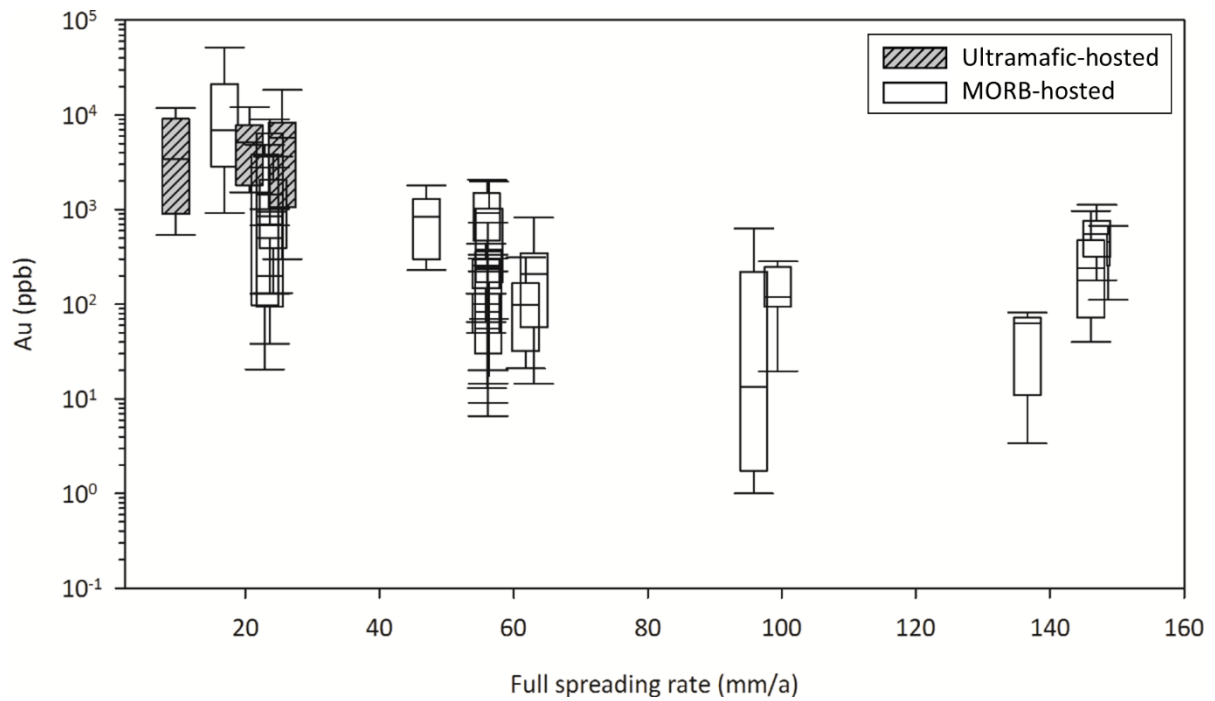
Figure 2





625  
 626  
 627  
 628  
 629

Figure 3



630  
 631  
 632

633

634

635

636

637

638

639

640

641

642

643

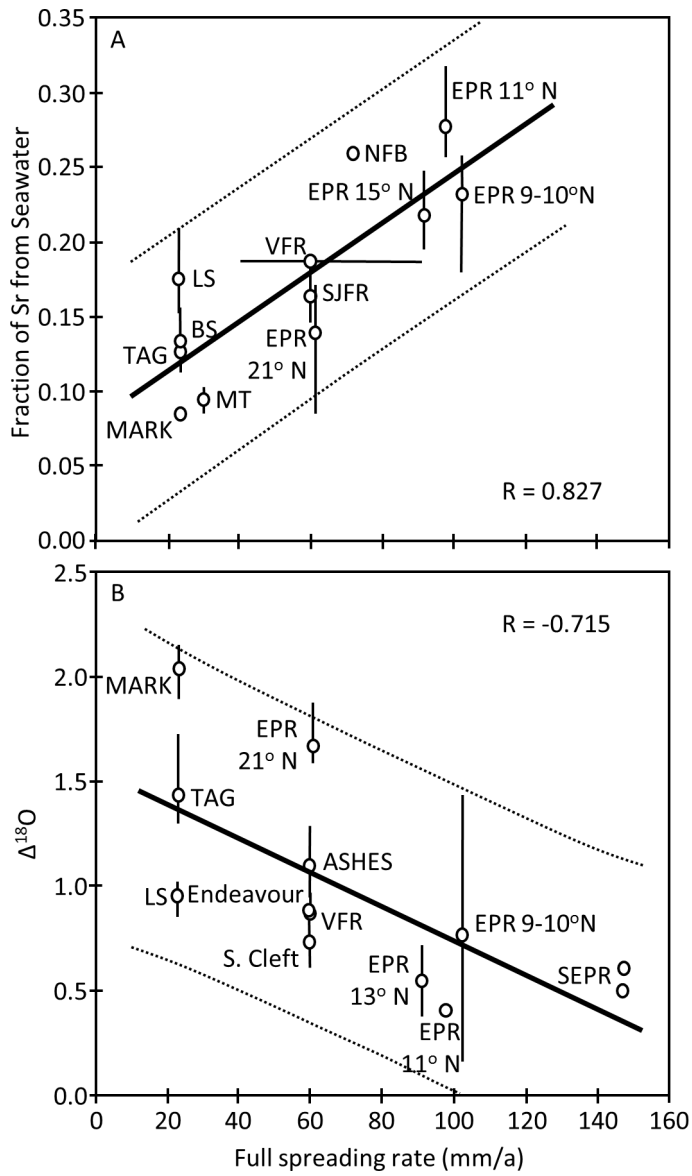
644

645

646

647

648 Figure 4



649

650

651

652

653

654

655

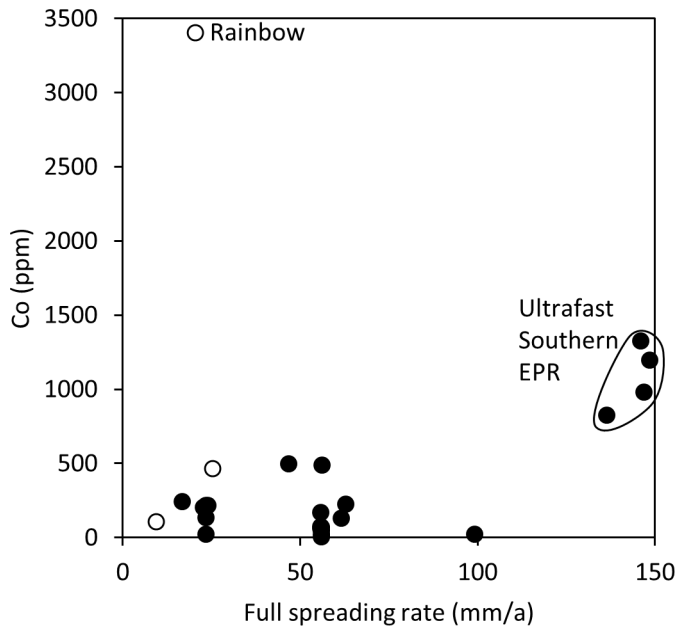
656

657

658

659

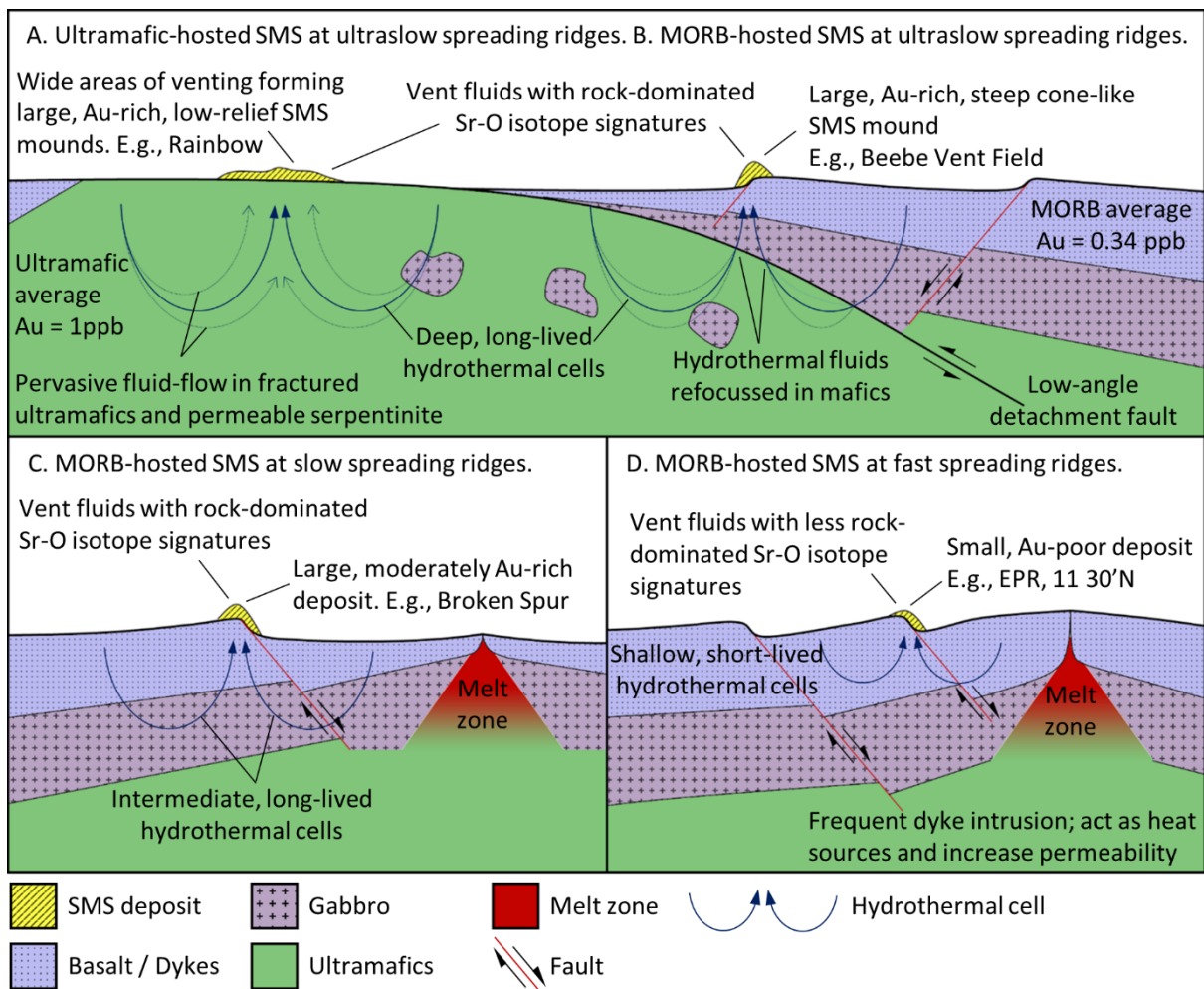
660 Figure 5



661

662

663 Figure 6



664